AIP Conference Proceedings

Vibrational frequencies and electronic structures of 2-amino-1, 9-dihydro-9-[(2-hydroxuethoxy) methyl]-6H-purin-6-one using density functional theory method

Cite as: AIP Conference Proceedings **2157**, 020010 (2019); https://doi.org/10.1063/1.5126545
Published Online: 18 September 2019

Suh-Miin Wang, Lee Muei Chng, Montha Meepripruk, and Pek-Lan Toh

View Online Export Citation

© 2019 Author(s).

Vibrational Frequencies and Electronic Structures of 2-amino-1, 9-dihydro-9-[(2-hydroxuethoxy) methyl]-6H-purin-6-one using Density Functional Theory Method

Suh-Miin Wang[1], Lee Muei Chng[1], Montha Meepripruk[2], Pek-Lan Toh[1*]

[1]*Faculty of Engineering and Green Technology, Universiti Tunku Abdul Rahman, Malaysia*
[2]*Institute of Science and Technology, Kampheang Phet Rajabhat University, Thailand*

[*]Corrsponding author: tohpl@utar.edu.my

Abstract. In this study, Density Functional Theory (DFT) calculations were conducted on Acyclovir (ACV) hydrate molecular system with the chemical formula of $3[C_8H_{11}N_5O_3]\cdot 2[H_2O]$. Geometry optimization calculations were performed to find the equilibrium structure of $3[C_8H_{11}N_5O_3]\cdot 2[H_2O]$. The optimized geometries were used to find the electronic structures of title molecule, i.e. total energies, frontier molecular orbital energies, atomic charges, and others. The results show that all structural parameters obtained are close to that of experiment. The total energies of $3[C_8H_{11}N_5O_3]\cdot 2[H_2O]$ are -70355.92 eV and -70373.84 eV, respectively for DFT/B3LYP/6-31G** and DFT/B3LYP/6-311G** levels of calculations. Using the scheme of Mulliken population analysis (MPA), the highest positive charge was localised on the atom of C_{12}, while for natural atomic charge distribution, C_9 atom possesses the highest positive charge. Moreover, the results of vibrational frequencies computed with two different basis sets are close to each other. The computed vibrational frequencies are overall corresponded with the region in the literature studies.

INTRODUCTION

In recent years, the subject of drug polymorphism has become an essential part of drug development. Numerous experiments have been conducted on the polymorph drugs [1-10]. In 2015, Censi and Martino studied the stability and bioavailability on the anhydrous and solvated forms of polymorph drugs [8]. The bioavailability of several polymorph drugs were summarised and discussed in the studied. Nicoud *et al,* in 2018 reported the solubility results of three metastable polymorphs, such as paracetamol, chloramphenicol palmitate, and sulfathiazole using three types of experiments [10]. It was known that the different molecular configurations can be affected the physical and chemical properties, such as colour, solubility, stability, and others. For example, a monoclinic form of ACV was studied by Birnbaum *et al.* [1], and a triclinic form of ACV was presented by Suwinska *et al.* [2]. Birnbaum and his co-workers, in 1984 found that the monoclinic form of ACV contains three molecules of ACV and two water molecules. The lattice parameters obtained are a = 25.459Å, b = 11.282Å, c = 10.768Å, and β = 95.16°, respectively. While for Suwinska *et al.* studies, ACV also contains ACV and water molecules. In 2013, Montha and Kenneth also re-investigated the triclinic form of tricyclic ACV [6]. The findings are close to Suwinska *et al.* studies. ACV is one of the anti-viral drugs [1-7, 9]. It can help to treat Herpes simplex virus (i.e. HSV-1 and HSV-2) infections, i.e. cold sore, chickenpox, and shingles by inhibiting the replication of viral DNA. The polymorph drugs can change the physicochemical properties, i.e. stability, solubility, bioavailability, and dissolution rate [1-10]. However, previously literature studies for the electronic structures of $3[C_8H_{11}N_5O_3]\cdot 2[H_2O]$ have several limitations. To improve the better understanding of polymorphism features for ACV under the drug development and industrial pharmacy, a DFT method was employed to study the structural molecules and electronic properties of $3[C_8H_{11}N_5O_3]\cdot 2[H_2O]$ in this work.

COMPUTATIONAL METHODOLOGY

All DFT calculations were carried out using personal computer with the help Gaussian 09 program package [11]. A molecular system of $3[C_8H_{11}N_5O_3]\cdot 2[H_2O]$ was used as the host environment in this work. Figure

International Symposium on Green and Sustainable Technology (ISGST2019)
AIP Conf. Proc. 2157, 020010-1–020010-9; https://doi.org/10.1063/1.5126545
Published by AIP Publishing. 978-0-7354-1902-5/$30.00

1 shows the molecular structure view of 3[$C_8H_{11}N_5O_3$].2[H_2O]. For the geometry optimization calculations, Becke's Three Lee-Yang-Parr (B3LYP) functional with 6-31G** and 6-311G** basis sets were chosen. The optimized geometry structures and electronic properties were then obtained. In addition, the surface plots of HOMO, LUMO, and molecular electrostatic potential (MEP) were also illustrated using GaussView 5.0 and Multiwfn software package [11-12].

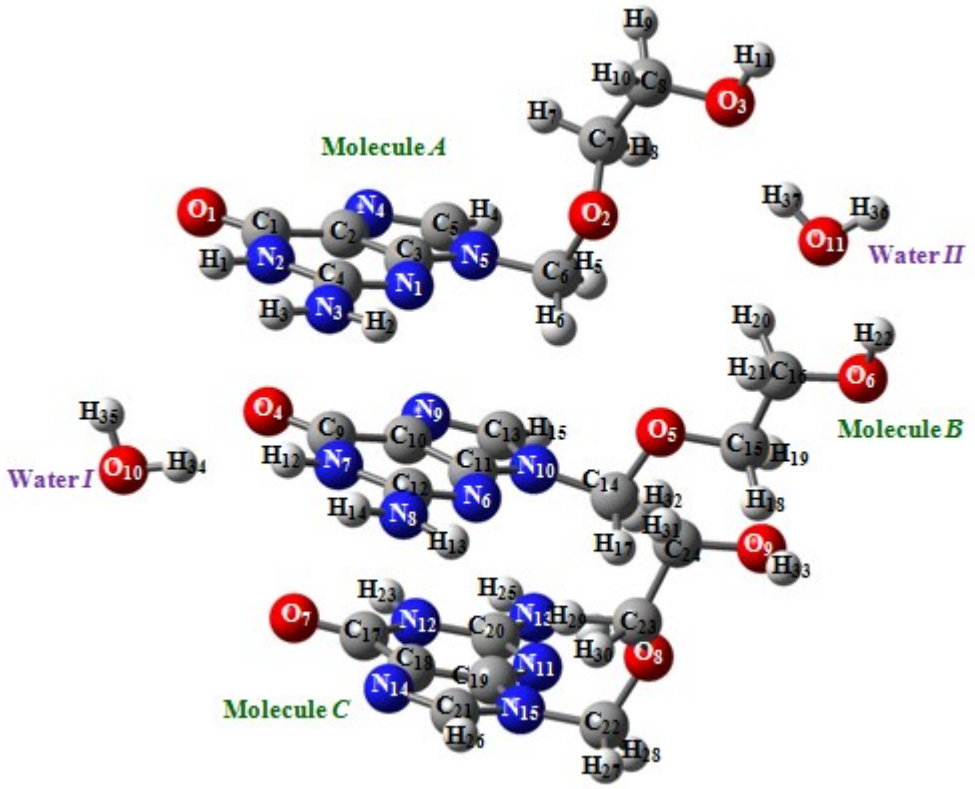

Figure 1. Molecular structure view of 3[$C_8H_{11}N_5O_3$]·2[H_2O]

RESULT AND DISCUSSION

Table 1 shows the results of geometrical structures of 3[$C_8H_{11}N_5O_3$]·2[H_2O] using the hybrid B3LYP functional and two basis sets (i.e. 6-31G** and 6-311G**). Since our computational results are focused on isolated molecule, the comparison geometries between the computational data and experiment are presented in this work. From the results reported in the table, the results obtained from both DFT/B3LYP/6-31G** and DFT/B3LYP/6-311G** levels of calculations are almost identical. All computed geometries are very close with experimental values [9]. For example, the percentage difference between the overall computed C-O and experimental bond values are less than 2.9% in the molecular system. While for C-N bonds in [$C_8H_{11}N_5O_3$]·2[H_2O], the percentage difference between the calculated data and experiment are less than 3.9%. In the case of bond angle, C-C-O possesses the highest percentage difference between the computational and experimental values, which is less than 6% in the molecular system. On the other hand, it was noted that all computed dihedral angles obtained from B3LYP/6-31G** and B3LYP/6-311G** technique are significantly closer to measurement data as shown in the table. From the optimised structure of 3[$C_8H_{11}N_5O_3$]·2[H_2O], the findings notice that there is no significantly change in the molecular system. Therefore, there is no further study on the geometry structures.

Table 2 gathers the computed total and Frontier molecular orbital energies of 3[$C_8H_{11}N_5O_3$]·2[H_2O]. Both of the results obtained from DFT/B3LYP/6-31G** and DFT/B3LYP/6-311G** levels of calculations show good agreement with each other. The total energy of 3[$C_8H_{11}N_5O_3$]·2[H_2O] obtained from B3LYP/6-31G** method is -70355.92 eV, whereas the value of -70373.84 eV is found for DFT/B3LYP/6-311G** level of calculation. To understand the details of chemical reactivity, electron transport mechanism, and stability of 3[$C_8H_{11}N_5O_3$]·2[H_2O], the values of HOMO-LUMO gaps in Table 2 and Figure 2 are determined to be about 5.01 eV and 4.91 eV, respectively for B3LYP functional with employing 6-31G** and 6-311G** basis sets. Moreover, the dipole

moments of 14.82 debye is obtained from DFT/B3LYP/6-31G** level of theory, whereas for B3LYP/6-311G** method, the dipole moments of $3[C_8H_{11}N_5O_3]\cdot 2[H_2O]$ is determined to be about 14.60 debye. The details of Frontier molecular orbitals (FMOs) are studied in this work. It was found that the diagrams obtained from the functional of B3LYP with two basis sets of 6-31G** and 6-311G** are close to each other. In Figure 3, the diagrams of Frontier molecular orbitals are illustrated using B3LYP/6-31G** method. As can be seen from the diagrams, the electron density distribution of Lowest Unoccupied Molecular Orbital (LUMO) is mainly localised on the guanine group of molecules B and C. For Highest Occupied Molecular Orbital (HOMO), the distribution of electron density is focused on the guanine group of molecule A.

Table 1. Computed molecular geometries of $3[C_8H_{11}N_5O_3]\cdot 2[H_2O]$

Molecule A	B3LYP/6-31G**	B3LYP/6-311G**	Exp [9]	Molecule B	B3LYP/6-31G**	B3LYP/6-311G**	Exp [9]	Molecule C	B3LYP/6-31G**	B3LYP/6-311G**	Exp [9]
Bond Distance (Å)											
O_1-C_1	1.216	1.209	1.239	O_4-C_9	1.222	1.216	1.241	O_7-C_{17}	1.217	1.210	1.245
C_1-N_1	1.441	1.442	1.391	C_9-N_7	1.419	1.419	1.383	C_{17}-N_{12}	1.442	1.443	1.388
N_2-C_4	1.372	1.370	1.375	N_7-C_{12}	1.375	1.373	1.372	N_{12}-C_{20}	1.366	1.364	1.368
N_1-C_3	1.361	1.359	1.353	N_6-C_{11}	1.357	1.355	1.339	N_{11}-C_{19}	1.356	1.353	1.348
C_3-C_2	1.393	1.390	1.375	C_{11}-C_{10}	1.391	1.389	1.392	C_{19}-C_{18}	1.394	1.392	1.375
C_4-N_3	1.369	1.369	1.335	C_{12}-N_8	1.361	1.361	1.336	C_{20}-N_{13}	1.362	1.362	1.336
C_2-N_4	1.380	1.378	1.387	C_{10}-N_9	1.381	1.379	1.385	C_{18}-N_{14}	1.383	1.382	1.385
C_3-N_5	1.378	1.377	1.367	C_{11}-N_{10}	1.379	1.378	1.379	C_{19}-N_{15}	1.378	1.377	1.376
N_5-C_6	1.454	1.454	1.469	N_{10}-C_{14}	1.443	1.443	1.444	N_{15}-C_{22}	1.459	1.459	1.462
C_6-O_2	1.417	1.417	1.391	C_{14}-O_5	1.407	1.406	1.395	C_{22}-O_8	1.400	1.399	1.408
O_2-C_7	1.420	1.421	1.428	O_5-C_{15}	1.429	1.430	1.424	O_8-C_{23}	1.429	1.429	1.435
C_7-C_8	1.508	1.505	1.490	C_{15}-C_{16}	1.510	1.507	1.460	C_{23}-C_{24}	1.502	1.500	1.499
C_8-O_3	1.426	1.428	1.419	C_{16}-O_6	1.410	1.411	1.391	C_{24}-O_9	1.426	1.427	1.421
Bond Angle (°)											
O_1-C_1-N_2	119.53	119.66	120.02	O_4-C_9-N_7	122.24	122.12	120.03	O_7-C_{17}-N_{12}	117.97	118.23	120.10
O_1-C_1-C_2	130.96	130.90	128.39	O_4-C_9-C_{10}	127.20	127.46	127.73	O_7-C_{17}-C_{18}	132.71	132.54	128.23
N_3-C_4-N_1	118.96	119.09	119.36	N_8-C_{12}-N_6	119.39	119.51	120.66	N_{13}-C_{20}-N_{11}	119.01	119.08	119.67
C_4-N_1-C_3	112.69	112.94	112.23	C_{12}-N_6-C_{11}	113.02	113.20	112.32	C_{20}-N_{11}-C_{19}	112.51	112.78	112.29
C_3-C_2-N_4	111.18	111.11	110.40	C_{11}-C_{10}-N_9	111.55	111.43	110.74	C_{19}-C_{18}-N_{14}	110.77	110.68	110.90
C_3-N_5-C_5	105.47	105.48	105.94	C_{11}-N_{10}-C_{13}	105.76	105.77	106.72	C_{19}-N_{15}-C_{21}	105.56	105.56	106.17
C_3-N_5-C_6	127.78	127.64	126.28	C_{11}-N_{10}-C_{14}	129.81	129.81	126.87	C_{19}-N_{15}-C_{22}	125.24	125.33	125.62

Table 1 continued

N_5-C_6-O_2	112.55	112.47	112.21	N_{10}-C_{14}-O_5	107.04	107.15	109.26	N_{15}-C_{22}-O_8	113.24	113.45	111.52
O_2-C_7-C_8	110.85	110.97	109.86	O_5-C_{15}-C_{16}	104.25	104.47	110.55	O_8-C_{23}-C_{24}	115.79	115.89	109.44
C_7-C_8-O_3	111.10	111.34	109.38	C_{15}-C_{16}-O_6	110.45	110.43	109.89	C_{23}-C_{24}-O_9	111.69	111.73	113.22
Dihedral Angle (°)											
O_1-C_1-C_2-C_3	179.88	179.88	179.88	O_4-C_9-C_{10}-C_{11}	-178.06	-178.06	-178.06	O_7-C_{17}-C_{18}-C_{19}	-178.36	-178.36	-178.36
O_1-C_1-N_2-C_4	179.39	179.39	179.4	O_4-C_9-N_7-C_{12}	-179.02	-179.02	-179.03	O_7-C_{17}-N_{12}-C_{20}	178.52	178.52	178.49
N_3-C_4-N_1-C_3	179.59	179.59	179.59	N_8-C_{12}-N_6-C_{11}	-178.37	-178.37	-178.37	N_{13}-C_{20}-N_{11}-C_{19}	177.51	177.51	177.51
N_1-C_3-N_5-C_6	-1.87	-1.87	-1.87	N_6-C_{11}-N_{10}-C_{14}	3.44	3.44	3.38	N_{11}-C_{19}-N_{15}-C_{22}	4.11	4.11	4.1
C_3-C_2-N_4-C_5	-0.24	-0.24	-0.24	C_{11}-C_{10}-N_9-C_{13}	-0.05	-0.05	-0.06	C_{19}-C_{18}-N_{14}-C_{21}	-0.52	-0.51	-0.52
N_5-C_6-O_2-C_7	-66.29	-66.29	-66.29	N_{10}-C_{14}-O_5-C_{15}	-173.34	-173.34	-173.34	N_{15}-C_{22}-O_8-C_{23}	76.85	76.85	76.85
O_2-C_7-C_8-O_3	73.51	73.51	73.51	O_5-C_{15}-C_{16}-O_6	-174.34	-174.34	-174.34	O_8-C_{23}-C_{24}-O_9	-60.56	-60.56	-60.56

Table 2. Total energies, Frontier molecular orbital energies, and dipole moments of $3[C_8H_{11}N_5O_3]\cdot 2[H_2O]$

	B3LYP/6-31G**	B3LYP/6-311G**
Total energy	-70355.92 eV	-70373.84 eV
HOMO	-5.25 eV	-5.48 eV
LUMO	-0.24 eV	-0.57 eV
HOMO-LUMO Gap	5.01 eV	4.91 eV
Dipole Moment	14.82 debye	14.60 debye

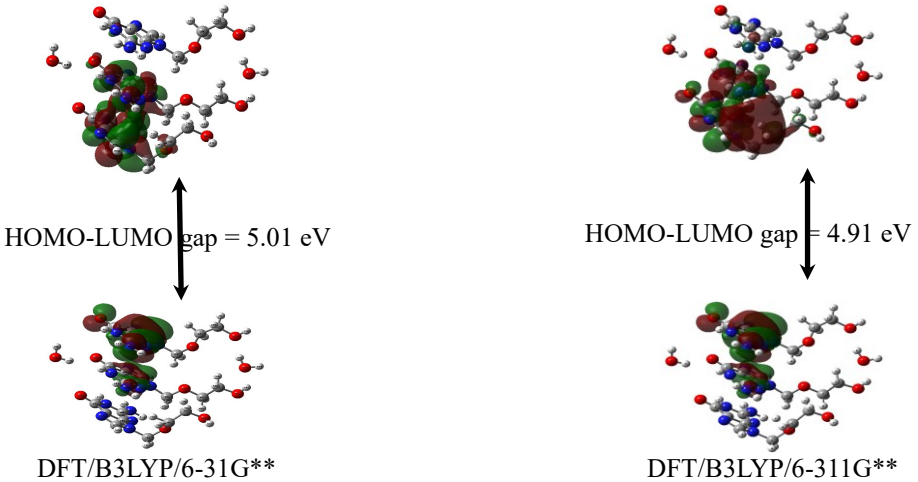

Figure 2: HOMO-LUMO energy gaps of $3[C_8H_{11}N_5O_3]\cdot 2[H_2O]$.

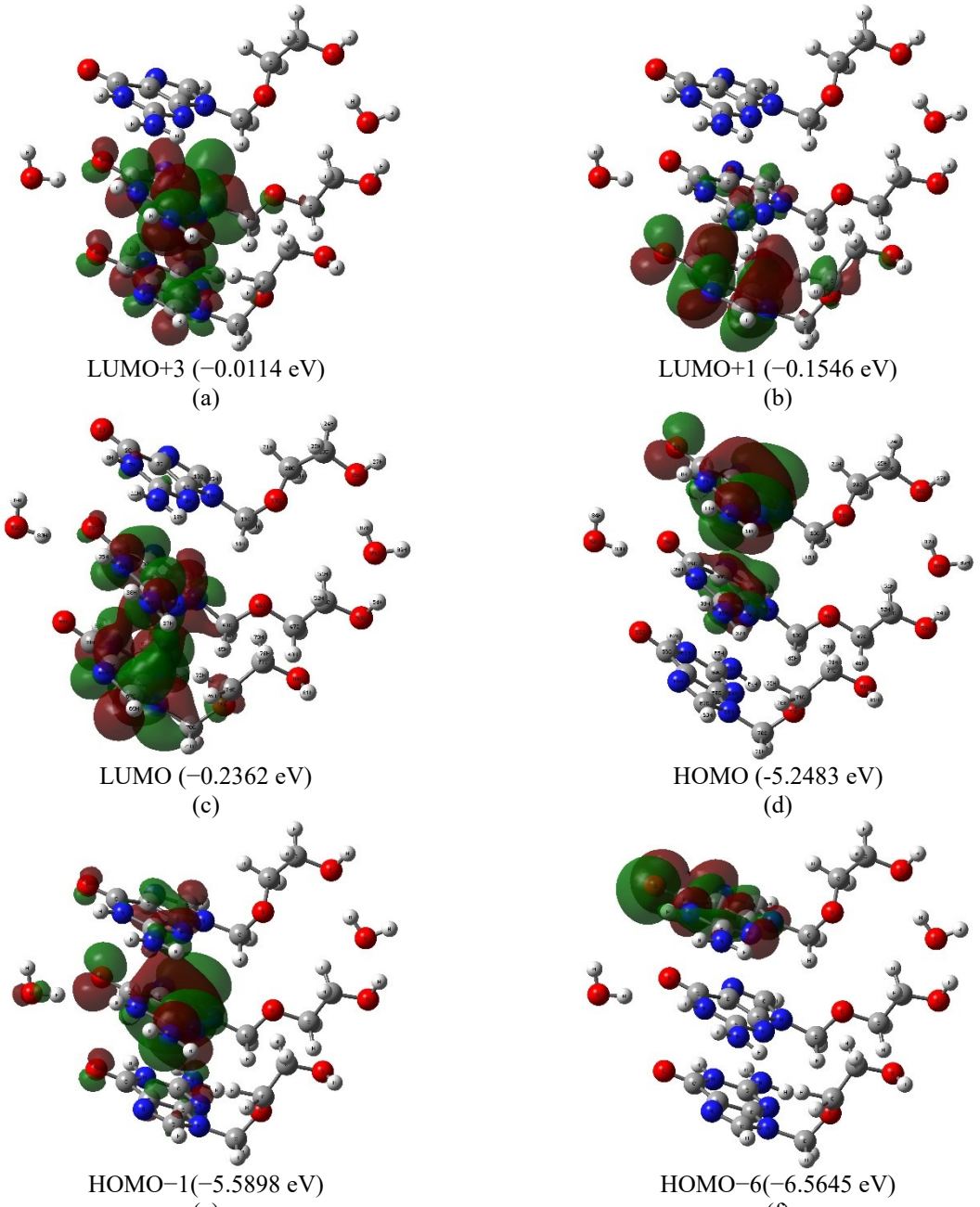

LUMO+3 (−0.0114 eV) (a)

LUMO+1 (−0.1546 eV) (b)

LUMO (−0.2362 eV) (c)

HOMO (-5.2483 eV) (d)

HOMO−1(−5.5898 eV) (e)

HOMO−6(−6.5645 eV) (f)

Figure 3. Frontier molecular orbital diagrams of $3[C_8H_{11}N_5O_3]\cdot 2[H_2O]$ using DFT/B3LYP/6-31G** level of calculation

The results of Mulliken and natural atomic charge distributions of $3[C_8H_{11}N_5O_3]\cdot 2[H_2O]$ are listed in Table 3. From the table, it can be noted that the charge values obtained from both of DFT/B3LYP/6-31G** and DFT/B3LYP/6311G** levels of theories are close to each other. For the distribution of Mulliken atomic charge, the highest positive charge is located on C_{12} atom, while the atom of C_9 is found using natural population analysis (NPA) scheme. All atoms of O and N possess the negative charge values. While the positive charges fall on H atoms as shown in the table. Moreover, the surface maps of molecular electrostatic potentials are presented in Figure 4 using B3LYP functional with the two different basis sets of 6-31G** and 6-311G**. Both of basis sets present the same MEP surface plot. From the diagram, the region of red colour shows the negative electrostatic potential in the molecular system, and the positive electrostatic potential falls in the region of blue colour. Also, the diagrams show the locations of global surface maximum and minimum for the methods of B3LYP/6-31G** and B3LYP/6-311G**. The red dot presents the global maximum on the surface, which is localised around the atoms of N_7 and N_8 in the guanine ring of molecule B, with the corresponding energetics of 2.57 eV and 2.55 eV,

respectively obtained from DFT/B3LYP/6-31G** and DFT/B3LYP/6311G** levels of calculations. While the location of global minimum (blue dot) is closest to the atom of O_{10} in the water I molecule. with the same energy value of -3.06 eV for 6-31G** and 6-311G** basis sets, respectively. The computed MEP plots can be used to understand the atomic charge distribution of $3[C_8H_{11}N_5O_3]\cdot 2[H_2O]$, and also the charge transfer within the molecular system in this study. Furthermore, the results of MEP plots obtained from two different basis sets show good agreement with the Mulliken and natural population analyses.

Table 3. Mulliken and natural atomic charge distributions of $3[C_8H_{11}N_5O_3]\cdot 2[H_2O]$

Molecule A	B3LYP/6-31G**		B3LYP/6-311G**		Molecule B	B3LYP/6-31G**		B3LYP/6-311G**		Molecule C	B3LYP/6-31G**		B3LYP/6-311G**	
	MPA	NPA	MPA	NPA		MPA	NPA	MPA	NPA		MPA	NPA	MPA	NPA
O1	-0.504	-0.588	-0.331	-0.589	**O4**	-0.542	-0.624	-0.389	-0.631	**O7**	-0.496	-0.578	-0.319	-0.579
C1	0.582	0.666	0.427	0.671	**C9**	0.626	0.671	0.485	0.673	**C17**	0.572	0.656	0.419	0.661
C2	0.146	-0.040	-0.101	-0.041	**C10**	0.126	-0.047	-0.145	-0.047	**C18**	0.132	-0.051	-0.129	-0.051
C3	0.502	0.350	0.332	0.363	**C11**	0.532	0.361	0.376	0.375	**C19**	0.537	0.366	0.390	0.379
N1	-0.594	-0.586	-0.413	-0.599	**N6**	-0.613	-0.588	-0.437	-0.604	**N11**	-0.615	-0.602	-0.432	-0.615
C4	0.734	0.628	0.577	0.641	**C12**	0.797	0.654	0.638	0.666	**C20**	0.755	0.640	0.592	0.652
N2	-0.625	-0.668	-0.485	-0.638	**N7**	-0.624	-0.645	-0.470	-0.614	**N12**	-0.614	-0.659	-0.474	-0.629
H1	0.265	0.435	0.223	0.399	**H12**	0.270	0.439	0.226	0.404	**H23**	0.284	0.449	0.242	0.413
N3	-0.677	-0.867	-0.520	-0.800	**N8**	-0.667	-0.843	-0.500	-0.776	**N13**	-0.665	-0.853	-0.502	-0.784
H2	0.291	0.437	0.244	0.402	**H13**	0.283	0.428	0.233	0.393	**H24**	0.294	0.438	0.248	0.403
H3	0.271	0.418	0.228	0.383	**H14**	0.273	0.420	0.224	0.385	**H25**	0.284	0.427	0.238	0.391
N4	-0.487	-0.435	-0.288	-0.441	**N9**	-0.492	-0.444	-0.282	-0.451	**N14**	-0.496	-0.447	-0.296	-0.453
C5	0.277	0.194	0.169	0.234	**C13**	0.254	0.181	0.132	0.219	**C21**	0.248	0.172	0.127	0.209
N5	-0.520	-0.437	-0.405	-0.437	**N10**	-0.525	-0.419	-0.386	-0.417	**N15**	-0.514	-0.437	-0.402	-0.437
H4	0.109	0.225	0.100	0.187	**H15**	0.105	0.224	0.095	0.187	**H26**	0.105	0.220	0.106	0.183
C6	0.183	0.073	0.125	0.163	**C14**	0.214	0.083	0.145	0.164	**C22**	0.164	0.070	0.115	0.166
H5	0.114	0.219	0.121	0.173	**H16**	0.082	0.204	0.084	0.158	**H27**	0.109	0.212	0.117	0.165
H6	0.152	0.261	0.154	0.212	**H17**	0.150	0.244	0.162	0.203	**H28**	0.147	0.257	0.142	0.205
O2	-0.479	-0.576	-0.364	-0.574	**O5**	-0.511	-0.605	-0.396	-0.603	**O8**	-0.451	-0.558	-0.333	-0.563

Table 3 continued

C7	0.060	-0.146	-0.028	-0.054	**C15**	0.040	-0.130	-0.035	-0.039	**C23**	0.057	-0.231	-0.033	-0.140
H7	0.111	0.223	0.123	0.176	**H18**	0.127	0.222	0.129	0.177	**H29**	0.053	0.228	0.065	0.184
H8	0.094	0.209	0.092	0.163	**H19**	0.084	0.198	0.094	0.151	**H30**	0.099	0.253	0.086	0.219
C8	0.030	-0.123	-0.007	-0.021	**C16**	0.082	-0.114	0.013	-0.014	**C24**	0.024	-0.138	-0.031	-0.046
H9	0.096	0.213	0.098	0.163	**H20**	0.067	0.189	0.071	0.143	**H31**	0.080	0.208	0.092	0.161
H10	0.115	0.219	0.115	0.169	**H21**	0.103	0.213	0.100	0.167	**H32**	0.151	0.239	0.157	0.190
O3	-0.538	-0.775	-0.424	-0.753	**O6**	-0.571	-0.774	-0.424	-0.744	**O9**	-0.518	-0.750	-0.378	-0.721
H11	0.319	0.493	0.254	0.460	**H22**	0.315	0.495	0.234	0.469	**H33**	0.305	0.478	0.233	0.448

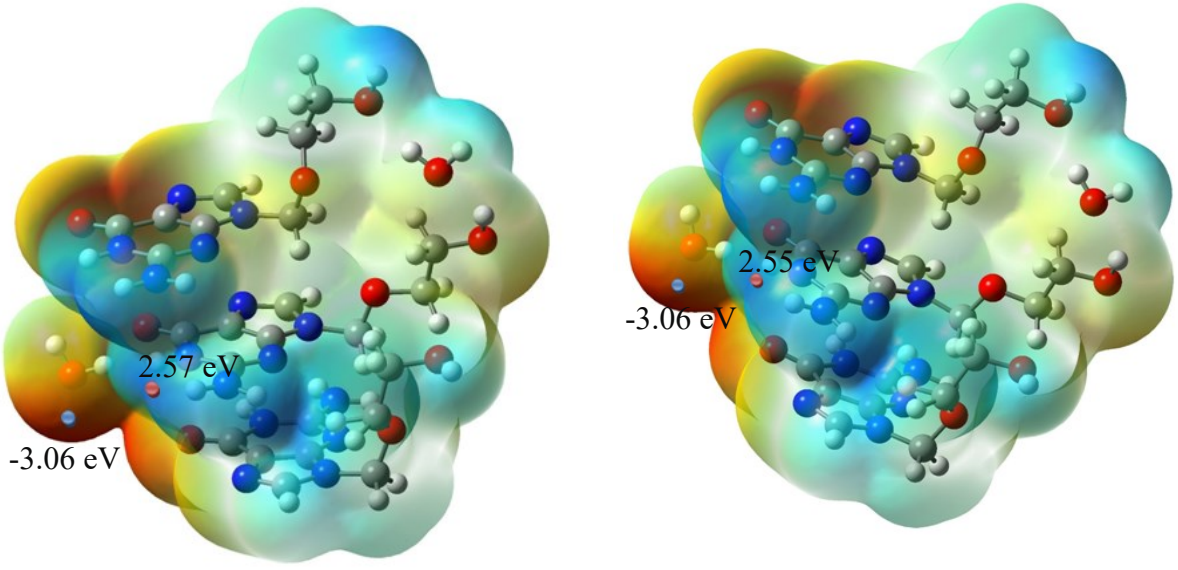

DFT/B3LYP/6-31G** (a) DFT/B3LYP/6-311G** (b)

Figure 4. Computed MEP surface plots of $3[C_8H_{11}N_5O_3]\cdot 2[H_2O]$ molecular system

There are no reported experimental findings on the different vibration modes of $3[C_8H_{11}N_5O_3]\cdot 2[H_2O]$ molecular system. To study the infrared spectroscopic signature of title molecule, the DFT computational calculations are conducted on the vibrational frequency analysis. The results in Table 4 presents the vibrational frequencies (i.e. unscaled and scaled) of $3[C_8H_{11}N_5O_3]\cdot 2[H_2O]$ molecular system using B3LYP method with two different basis sets (i.e. 6-31G** and 6-311G**). The scale factors used are 0.961 and 0.967, respectively for B3LYP/6-31G** and B3LYP/6-311G** techniques. The molecular structure of $3[C_8H_{11}N_5O_3]\cdot 2[H_2O]$ has the space group of $P2_1/n$, consists 87 atoms in the system. Therefore, it has 19 out of 255 normal vibrational modes, which can be distributed as 10 types of vibrations. The calculated vibrational frequencies either unscaled or scaled obtained from DFT/B3LYP/6-31G** and DFT/B3LYP/6-311G** levels of theories show good agreement with the recorded spectral in the literature data [4]. For $3[C_8H_{11}N_5O_3]\cdot 2[H_2O]$ molecular system, the O-H stretching vibrations are found at 3669 cm^{-1} (unscaled) and 3526 cm^{-1} (scaled) in the molecular system using DFT/B3LYP/6-31G** level of theory. Similar to B3LYP/6-311G** results, the peaks are observed at 3673 cm^{-1}

(unscaled) and 3552 cm^{-1} (scaled). The N-H stretching vibrations for B3LYP functional with the basis set of 6-31G** are appeared at 3639 cm^{-1} (unscaled), 3597 cm^{-1} (unscaled), 3497 cm^{-1} (scaled), and 3456 cm^{-1} (scaled). Similarly, the bands obtained from B3LYP/6-311G** technique are occurred at 3626 cm^{-1} (unscaled), 3589 cm^{-1} (unscaled), 3506 cm^{-1} (scaled), and 3471 cm^{-1} (scaled). For B3LYP/6-31G** method, the overall vibrational frequencies (i.e. unscaled and scaled) obtained are close to that of DFT/B3LYP/6-311G level of calculation. For example, the H-C-H stretching vibrations are located in the range of 3233 cm^{-1} - 2876 cm^{-1} and 1443 cm^{-1} - 1386 cm^{-1}. Moreover, the bands occurred at the ranges of 1805 cm^{-1} - 1727 cm^{-1} and 1593 cm^{-1} - 1466 cm^{-1} have been assigned to the C=O and C=C stretching vibrations in $3[C_8H_{11}N_5O_3]\cdot 2[H_2O]$ system. In this study, all the computed stretching and bending vibrational frequencies are presented within the region of molecular system.

Table 4. Computed vibrational frequencies (cm^{-1}) of $3[C_8H_{11}N_5O_3]\cdot 2[H_2O]$ molecular system

	DFT/B3LYP/6-31G**		DFT/B3LYP/6-311G**	
Type of Vibration	**Unscaled**	**Scaled**	**Unscaled**	**Scaled**
O-H stretching vibration	3669	3526	3673	3552
N-H stretching vibration	3639	3497	3626	3506
N-H stretching vibration	3597	3456	3589	3471
H-C-H stretching vibration	3192	3068	3233	3127
H-C-H stretching vibration	2993	2876	2981	2883
C=O stretching vibration	1805	1735	1786	1727
C=C stretching vibration	1593	1531	1590	1537
C=C stretching vibration	1526	1466	1519	1469
H-C-H bending vibration	1443	1386	1443	1395
C-N stretching vibration	1406	1351	1397	1351
C-N stretching vibration	1365	1311	1358	1313
C-O-C stretching vibration	1254	1205	1256	1214
C-O stretching vibration	1136	1091	1137	1100
C-O stretching vibration	1124	1080	1125	1088
C-O stretching vibration	1075	1033	1072	1037
C-O stretching vibration	1064	1022	1057	1023
C-H bending vibration	863	829	862	833
C-H bending vibration	813	781	815	788
C-H bending vibration	801	770	794	768

CONCLUSION

In this work, the geometry and electronic structures of $3[C_8H_{11}N_5O_3]\cdot 2[H_2O]$ were investigated using DFT quantum mechanical computational method. For $3[C_8H_{11}N_5O_3]\cdot 2[H_2O]$ molecular system, the results obtained from B3LYP/631G** and B3LYP/6311G** levels of calculations show good agreement with experimental results in terms of geometrical parameters (bond distances, bond angles, and dihedral angles) [1]. The total energy obtained from B3LYP/6-31G** method is -70355.92 eV, while the total energy value of -70373.84 eV is found at DFT/B3YP/6-311G** level of theory. For B3YP/6-31G** technique, the vibrational frequencies obtained are close to the findings of 6-311G** basis set. The overall computed vibrational frequencies are found within the region in the literature [4]. These theoretical results will provide the fundamental knowledge of ACV at the microscopic level. Also, it can use to complement the experimental studies.

ACKNOWLEDGMENTS

The authors would like to thank Universiti Tunku Abdul Rahman and UTARRF grant.

REFERENCES

1. G. I. Birnbaum, M. Cygler and D. Shugar, *Canadian journal of chemistry* **62(12)**, pp. 2646-2652 (1984).
2. K. Suwińska, B. Golankiewicz and W. Zielenkiewicz, *Acta Crystallographica Section C: Crystal Structure Communications* **57(6)**, pp. 767-769 (2001).
3. Y. T. Sohn, and S. H. Kim, *Archives of Pharmacal Research* **31(2)**, pp. 231-234 (2008).
4. K. M. Lutker, R. Quinones, J. Xu, A. Ramamoorthy and A. J. Matzger, Journal of Pharmaceutical Sciences **100(3)**, pp. 949-963 (2011).
5. T. Masuda, Y. Yoshihashi, E. Yonemochi, K. Fujii, H. Uekusa and K. Terada, *International Journal of Pharmaceutics* **422(1-2)**, pp. 160-169 (2012).
6. M. Montha and J. H. Kenneth, *Acta Crystallographica Section C: Crystal Structure Communications* **69(9)**, pp. 1077-1080 (2013).
7. A. Sarkar and S. Rohani, *Journal of Pharmaceutical Sciences* ***104*****(1)**, pp. 98-105(2015).
8. R. Censi and P. D. Martino, *Molecules*, **20**, pp. 18759-18776 (2015).
9. Q. Cai, J. Xue, Q. Wang and Y. Du, *Spectrochimica Acta Part A: Molecular and Biomolecular Spectroscopy* **186**, pp. 29-36 (2017).
10. L. Nicoud, F. Licordari and A. S. Myerson, *Crystal Growth & Design* **18(11)**, pp. 7228-7237 (2018).
11. M. J. Frisch, G. W. Trucks, H. B. Schlegel, G. E. Scuseria, M. A. Robb and J. R. Cheeseman, GAUSSIAN09, Revision E. 01. Gaussian Inc., Wallingford, CT, USA. (2009)
12. T. Lu and F. Chen, *Journal of Computational Chemistry* **33(5)**, pp. 580-592 (2012).